Journal of Materials Chemistry B

PAPER

View Article Online
View Journal

Cite this: DOI: 10.1039/d0tb00507j

Unique sequence-dependent properties of trinucleotide repeat monolayers: electrochemical, electrical, and topographic characterization†

Narges Asefifeyzabadi,[a] Motahareh Taki,[a] Madison Funneman,[a] Tingjie Song[b] and Mohtashim Hassan Shamsi *[a]

Received 24th February 2020,
Accepted 3rd May 2020

DOI: 10.1039/d0tb00507j

rsc.li/materials-b

Trinucleotide repeat (TNR) sequences widely exist in nature and their overgrowth is associated with two dozen neurodegenerative diseases in humans. These sequences have a unique helical flexibility, which affects their biophysical properties. A number of biophysical properties of these sequences have been studied in the past except their surface-tethered monolayers. To address the effect of sequence context and the associated helical flexibility on TNR monolayers, disease-relevant TNRs from three flexibility groups were surface-assembled on gold surfaces. The properties of the TNR films were studied, including charge transfer resistance (R_{ct}) by electrochemical impedance spectroscopy (EIS), surface density by chronocoulometry (CC), surface topography by atomic force microscopy (AFM), and electrical conductivity by conducting atomic force microscopy (C-AFM). We found that the TNR film properties are characteristically sequence dependent rather than being dependent on their flexibility rank reported in the literature. The characteristic properties of TNR films studied here may be used for engineering label-free biosensors to detect neurological disorders and build DNA bioelectronics.

1. Introduction

DNA repeat sequences such as trinucleotide repeat (TNR) are a class of short nucleic acid sequences that repeat sporadically and in tandem across living organisms. In humans, some TNRs have been associated with over two dozen genetically transferrable neuromuscular and neurodegenerative diseases.[1,2] At the molecular level, the repetition of TNR combinations leads to a certain sequence-directed flexibility that allows them to form unique secondary structures.[3,4] Theoretical calculations based on helical parameters have classified 64 possible TNR combinations into 12 groups of flexibilities.[5] In contrast to a random sequence, the persistence lengths of some TNRs were reported to be 40% shorter than that of normal B-DNA having a 50 nm persistence length.[6] Moreover, the presence of only four TNR repeats in a sequence may introduce flexibility in the helical structure similar to the flexibility caused by a dinucleotide T–T mismatch.[7]

A few disease specific TNRs (CGG, CTG, CAG, and GAA) have been widely characterized by a range of techniques including electrophoresis,[8,9] mass spectroscopy,[10] circular dichroism,[11] nuclear magnetic resonance,[12,13] optical melting study and differential scanning calorimetry,[14,15] and recently by a pump-free wax-on-plastic microfluidics technique.[16] Nevertheless, TNR-based biointerfaces have not been characterized thus far. For biosensing and bioelectronic applications, the knowledge of DNA-based interfaces or surface-assembled films is critical, such as surface densities, charge transport properties, electrostatics, molecular mechanics, stability of surface-tethered states, and interactions with the surface and neighbouring environment.[17]

Here, we report for the first time a systematic study on TNR surface-tethered monolayers. As depicted in Scheme 1, surface-tethered films may form unique monolayers owing to their sequence-directed helical parameters that may translate into unique electrochemical and surface–probe signals. To investigate the effects, we characterized the monolayers of three TNR sequences from three different flexibility groups on gold surfaces. The surface properties that were studied include charge transfer resistance (R_{ct}) by electrochemical impedance spectroscopy (EIS), surface density by chronocoulometry (CC), surface topography by atomic force microscopy (AFM), and electrical conductivity by conducting atomic force microscopy (C-AFM). The evidence of unique film properties of TNRs evolved from this study reinforces the efforts of developing label-free biosensors to detect DNA repeat expansion disorders and developing bioelectronic devices.[18]

[a] Department of Chemistry & Biochemistry, 1245 Lincoln Dr, Southern Illinois University at Carbondale, IL 62901, USA. E-mail: mshamsi@siu.edu
[b] Department of Chemistry, University of Illinois at Urbana-Champaign, IL 61801, USA

† Electronic supplementary information (ESI) available. See DOI: 10.1039/d0tb00507j

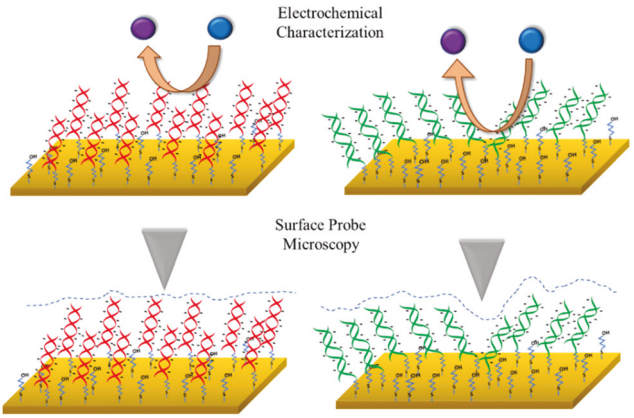

Scheme 1 The electrochemical and surface probe microscopic characterization of self-assemblies of rigid and flexible TNR sequences on gold surfaces. The TNR sequences were tethered to gold surfaces through a Au–S$(CH_2)_6$–DNA linkage and nonspecific binding was prevented by a filler layer of mercaptohexanol (MCH).

2. Experimental

2.1. Reagents and materials

$K_4[Fe(CN)_6]$, $K_3[Fe(CN)_6]$, sulfuric acid (98%), and sodium chloride were purchased from Thermo Fisher Scientific (Waltham, MA). Tris(hydroxymethyl)aminomethane (Tris–ClO_4), $Ru(NH_3)_6Cl_3$, 6-mercapto-1-hexanol (MCH) and magnesium chloride solution (1 M) were purchased from Sigma-Aldrich (St. Louis, MO). Gold disc electrodes and platinum wire electrodes were purchased from CH Instruments (Austin, TX). The Ag/AgCl reference electrodes and velvet cloth to polish electrodes were obtained from Bioanalytical Systems Inc. (West Lafayette, IN). The HPLC purified probe sequences with a 6-hydroxyhexyl disulfide group at the 5′ position and the complementary sequences were purchased from IDT (Integrated DNA Technologies, Coralville, IA). Template-stripped ultra-flat gold substrates were purchased from Platypus Technologies. Olympus tips, AC240TM, with platinum coating were used for topographic and conductivity measurements of atomic force microscopy (AFM).

2.2. Preparation of TNR solutions

To prepare 10 μM double-stranded TNR solutions, 20 μL aliquots of 20 μM OH$(CH_2)_6$–S–S–$(CH_2)_6$-modified base sequence solution and 20 μM solutions of the complementary sequences were mixed in a buffer (100 μM Tris buffer containing 20 mM $MgCl_2$ and 200 mM NaCl) with pH 8.5 and heated up to the melting temperatures of the TNRs for 30 minutes followed by annealing at room temperature for 1 hour and storing at 4 °C.

2.3. Preparing surface-tethered films of TNRs on gold electrodes

For electrochemical study, surfaces of gold working electrodes were regenerated by mechanical and electrochemical polishing. Briefly, gold disc electrodes of 2 mm diameter were polished with three different grain sizes of alumina powder (1, 0.3, and 0.05 μm) followed by 10 minutes sonication in DI water. Cyclic voltammetry was performed for electrochemical cleaning of the mechanically polished electrodes by running 20 cycles in 0.5 M H_2SO_4 with a potential range of 0–1.5 V against a Ag/AgCl reference electrode and a platinum wire counter electrode. The gold oxide stripping peak of the last cycle was used to measure the roughness factor of the electrodes that was kept as $\leq$1.2. The electrodes were preserved in a 1 : 1 ethanol : water mixture. Then, 10 μL of hybridized solutions of TNRs was dropped on the electrodes to form films on the freshly cleaned and polished gold surfaces at 4 °C. The electrodes were capped with Eppendorf tubes to prevent evaporation and incubated for 4 days according to our optimized condition,[18] where the disulfide bond in the presence of gold transforms into a thiol group spontaneously and attaches to the gold surface through the Au–S linkage.[19] Then, the modified electrodes were washed with buffer and further incubated in 1 mM mercaptohexanol for 30 minutes to block any unbound surface of the gold electrode and remove physically adsorbed DNA strands followed by another washing step.

2.4. Electrochemical measurements

All electrochemical experiments were performed on a CHI 660E (CHI, Austin, TX) electrochemical workstation at room temperature in a three-electrode cell with the modified gold electrodes as the working electrode (with the geometric area of 0.0314 cm^2), platinum wire as the counter electrode and Ag/AgCl as the reference electrode. Electrochemical impedance spectroscopy (EIS) was carried out on the double-stranded repeat sequences using a soluble redox probe, *i.e.* 1 mM $[Fe(CN)_6]^{3-/4-}$ prepared in 100 μM Tris buffer, pH 7.4. The following parameters were used to run the EIS measurements: Frequency range from 100 kHz to 1 Hz, an applied potential of 250 mV *vs.* Ag/AgCl, and an AC voltage of 5 mV amplitude. For simulation, Z-view version 3.5 d was used to fit the EIS data into Randle's equivalent circuit and to extract the values for charge transfer resistance (R_{ct}).

Tarlov's method was used to calculate the surface density of the TNR using chronocoulometry.[20] Briefly, this involves charge measurement on DNA modified electrode surfaces before and after exposure of DNA films to $Ru(NH_3)_6^{3+}$. In chronocoulometric study, a potential step was applied to the TNR modified electrodes followed by measuring the resulting charge *vs.* $(time)^{1/2}$ under an equilibrium condition in the absence and presence of 5 μM $[Ru(NH_3)_6]^{3+}$ prepared in 10 mM Tris–ClO_4 (pH 7.4). The chronocoulometric measurements were carried out with the pulse period of 500 ms, pulse width of 600 mV (from +150 mV to −450 mV) and quiet time of 30 s. Deoxygenation of the solution was performed by purging nitrogen gas through the buffer and redox marker solution for 30 minutes before measurement. Representative plots of CC measurements are shown in Fig. S1 in the ESI.†

2.5. Atomic force microscopy and conductivity measurements

Ultra-flat gold substrates were used for all AFM measurements and were washed with acetone and deionized water followed by rinsing with Tris buffer and finally drying under N_2. Then, 10 μM double-stranded TNR solutions as prepared above were

dropped on the surfaces of the clean gold substrates and incubated as mentioned above. Then, the surfaces were rinsed with the Tris buffer and dried under N_2 before AFM measurements. All AFM measurements were performed under air dry conditions using a Cypher S Asylum Research AFM Microscope, at the University of Illinois Urbana-Champaign. Olympus tips, with platinum coating, a spring constant of 2 N m^{-1}, a resonance frequency of 70 kHz and a tip radius of 15 nm were used. The open source imaging analysis software 'Gwyddion' was used for analysing the AFM images.[21] Topographic images with resolutions of 300 nm × 300 nm and 1 μm × 1 μm area were obtained in tapping mode on three replicate surfaces. The surface profiles were extracted from the images across the centre of each image. For electrical measurements by AFM, the sample was mounted on an AFM disc and Leitsilber silver paint was used to conductively glue the sample on the AFM disc. The conductivity measurements were made in contact mode, where the electrically conductive probe was scanned over the DC-biased TNR-modified surfaces. The current–potential (*I–V*) curves were obtained by single point measurement of the current as a function of voltage applied to the sample. Before recording current–voltage curves, an image was collected from the sample surface in AC mode and then measurements were made in contact mode and spectra were collected from the chosen spots. The setpoint potential of 0.1–0.5 V corresponding to 17–85 nN applied force was used to collect *I–V* curves between ±2 V applied potential.

3. Results and discussion

Based on the computational analysis of helical parameters, Baldi *et al.* classified 64 possible TNR sequences into 12 groups by designating a value to each TNR on a so-called 'flexibility scale'.[5] According to the computational model, the TNRs given in Table 1 are ranked in flexibility as CGG > CTG > GAA. Whereas, another report ranked these sequences as CTG > CGG ≈ GAA.[22] In this study, the prehybridized TNR duplexes were surface-tethered on cleaned and polished gold surfaces through a Au–S linkage followed by filling the residual space with mercaptohexanol (MCH) to prevent nonspecific adsorption of nucleobases on gold surfaces. First, the TNR-modified gold electrodes were characterized by EIS, which has been extensively used as a label-free macroscopic approach to detect structural distortion in DNA at the molecular level that manifests into distinct monolayers.[23–27] EIS was used to test the diffusion of a soluble redox probe, $Fe(CN)_6^{3-/4-}$, through the TNR films, where the diffusion is impeded by the electrostatic repulsion between the redox probe and negatively charged phosphate backbone of DNA along with physical resistance of the film. The EIS data were fit into the modified Randle's equivalent circuit (see Fig. S2 in the ESI†). The resistive and capacitance elements extracted by fitting the experimental data into the modified Randle's equivalent circuit are given in Table 2. Among all the circuit elements, charge transfer resistance (R_{ct}) was found to be a distinctive property with a lower standard error (RSD ∼ 10%) across the sequences, thus it was used to compare the sequences, as shown in Fig. 1. In the given frequency range, '*W*' was not completely pronounced leading to significantly higher error. It may be attributed to DNA monolayers are not uniform coating, therefore, diffusion may not be uniform across the surface at low frequencies.

Table 2 The average values of modified Randle's equivalent circuit elements for each double-stranded TNR sequence. The standard errors in parentheses were calculated for $N \geq 4$ separate measurements

	$R_s/\Omega\ cm^2$	$C_{dl}/F\ cm^{-2}\ (10^{-8})$	$R_{ct}/\Omega\ cm^2$	$W/\Omega\ cm^2$
Bare gold	0.32 (0.04)	356 (0.4)	138 (26)	1.6 (0.1) × 10^9
MCH	1.0 (0.35)	82 (47)	285 (60)	23 (10) × 10^6
CGG-8	0.04 (0.02)	6.4 (2.4)	3108 (193)	2750 (1508)
CCG-8	0.20 (0.05)	2.4 (0.2)	3128 (290)	1519 (437)
CTG-8	0.04 (0.01)	4.6 (0.6)	1497 (179)	514 (123)
CAG-8	0.19 (0.04)	6.0 (1.7)	1405 (183)	329 (741)
CAG-4	1.58 (0.80)	7.3 (5.9)	983 (98)	7 (4) × 10^6
GAA-8	0.07 (0.05)	2.5 (0.2)	1855 (75)	3312 (5312)
GAA-5	0.56 (0.15)	18.0 (5.4)	548 (54)	877 (625)
GAA-4	3.61 (0.69)	12.0 (2.6)	426 (70)	1219 (454)

Table 1 Description of the trinucleotide repeats with their complementary sequences

TNR type	Sequence[a]	Repeat length	Flexibility[b]
CGG-8	5′linker-CGG CGG CGG CGG CGG CGG CGG CGG-3′ 3′-GCC GCC GCC GCC GCC GCC GCC GCC-5′	8	Highly flexible
CCG-8	5′linker-CCG CCG CCG CCG CCG CCG CCG CCG-3′ 3′-GGC GGC GGC GGC GGC GGC GGC GGC-5′	8	
CAG-4	5′linker-CAG CAG CAG CAG-3′ 3′-GTC GTC GTC GTC-5′	4	Medium flexible
CAG-8	5′linker-CAG CAG CAG CAG CAG CAG CAG CAG-3′ 3′-GTC GTC GTC GTC GTC GTC GTC GTC-5′	8	
CTG-8	5′linker-CTG CTG CTG CTG CTG CTG CTG CTG-3′ 3′-GAC GAC GAC GAC GAC GAC GAC GAC-5′	8	
GAA-4	5′linker-GAA GAA GAA GAA-3′ 3′-CTT CTT CTT CTT-5′	4	Least flexible
GAA-5	5′linker-GAA GAA GAA GAA GAA-3′ 3′-CTT CTT CTT CTT CTT-5′	5	
GAA-8	5′linker-GAA GAA GAA GAA GAA GAA GAA GAA-3′ 3′-CTT CTT CTT CTT CTT CTT CTT CTT-5′	8	

[a] Linker molecule $OH(CH_2)_6$–S–S–$(CH_2)_6$–DNA. The disulfide bond in the presence of gold transforms into the thiol group spontaneously and attaches to the gold surface through the Au–S linkage. [b] See ref. 5.

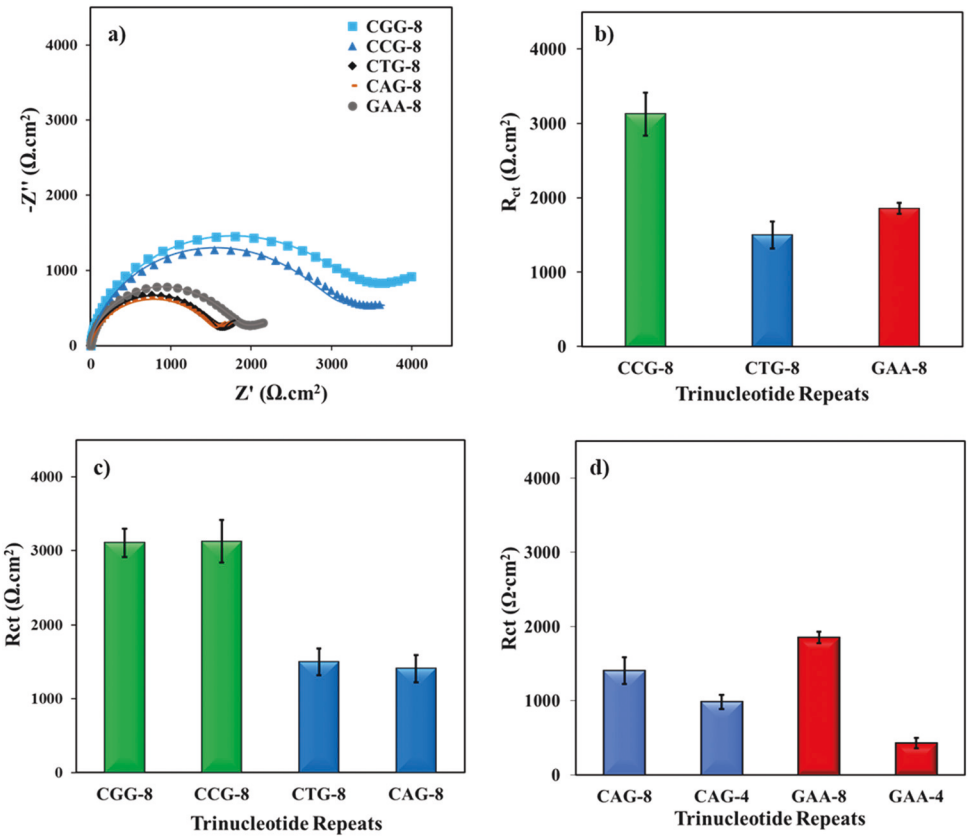

Fig. 1 (a) Representative Nyquist form of EIS plots of dsTNR-8 from the three flexibility groups. Markers show experimental data points and lines represent curve fits to the modified Randle's equivalent circuit. (b) Comparing the R_{ct} responses of representative dsTNR-8 sequences of the three groups, (c) comparing pairs of dsTNR-8 from the highest and medium flexibility groups, (d) comparing two different lengths, dsTNR-8 and dsTNR-4, from the medium and least flexibility group. Green = highest flexibility, blue = medium flexibility, and red = least flexibility group. Error bars represent the standard deviation of 4 replicate surfaces.

Fig. 1a shows representative curves of the Nyquist form of EIS plots for dsTNR-8 sequences. The EIS plots for bare gold and MCH modified gold surfaces are given in the ESI† (Fig. S3). In Fig. 1b–d, the bar graphs compare number of variables between the groups and within the groups (green = highest, blue = medium, and red = least flexible groups). Fig. 1b shows the comparison between representative dsTNR-8 sequences from the three flexibility groups. The results indicate that CCG-8, representing the highest flexibility, has the largest R_{ct} compared to the medium and least flexible sequences. All three groups show distinct resistive character but the higher R_{ct} of GAA-8 (least flexible) than that of CTG-8 (medium flexible) indicates that the electrochemical resistive property is dependent on sequence context and independent of rank on the flexibility scale. One may assume that switching the tethering strand in a duplex may cause a change in the resistive property. To assess the effect of the tethering strand, Fig. 1c compares dsTNR-8 from the highest flexibility and medium flexibility groups, where the pairs from each group are complementary to each other, *i.e.* CGG *vs.* GCC and CTG *vs.* CAG with the difference of tethering strand. It is evident that the R_{ct} responses of complementary TNR duplexes are indistinguishable from each other while a significant difference between the two groups still exists. This result suggests that for a biosensing application, any strand from a duplex can be used for surface immobilization to observe the overall resistive response of a repeat sequence. To investigate how the length of TNRs of different flexibilities affects their resistive property, medium and least flexibility groups with 8 and 4 repeat units were compared, as shown in Fig. 1d. The R_{ct} was lower for the shorter repeats in both groups due to the less negative charge and physical resistance, however the degree of change was much higher in the case of the least flexible GAA sequence (77% decrease) compared to medium flexible CAG (30% decrease). The results suggest that the degree of change in resistive properties with respect to length may also be sequence-dependent, which perhaps affects their monolayer structure, uniformity, and packing.

Surface coverage of TNRs may also be affected by their sequence context and flexibility. To investigate the effects, the surface densities were measured using Tarlov's method,[20] which relies on charge accumulation on a DNA modified surface due to the adsorption of $Ru(NH_3)_6^{3+}$ on the phosphate groups of the DNA film (see ESI† for the details of the method). The accumulated charge is correlated to the number of phosphate groups in the DNA monolayer and that can be converted into the

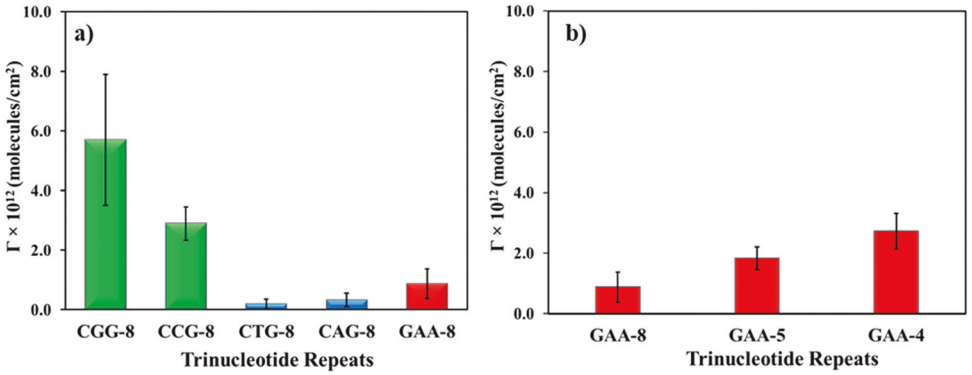

Fig. 2 (a) Surface densities of dsTNR-8 sequences of the three flexibility groups. (b) Surface densities of different lengths of dsGAA sequences. Green = highest flexibility, blue = medium flexibility, and red = least flexibility group. Error bars represent the standard deviation of 4 replicate surfaces.

number of DNA strands immobilized using the Cottrell equation. The results shown in Fig. 2a prove that the surface coverage of the three groups is distinguishable and affected by the type of TNR sequence similar to the resistive property shown above. With respect to length, GAA with 4, 5, and 8 repeats was tested and the surface density was found to decrease with the length (Fig. 2b), which is similar to a report on single-stranded DNA probe sequences.[28] Table S1 in the ESI† gives the surface density in number of strands ($\times 10^{12}$ molecules cm^{-2}), number of moles (pmol cm^{-2}), and the mass adsorbed (ng cm^{-2}) on the surface. Despite a decrease in the surface density with length, the R_{ct} for these sequences increased (see Table 2), confirming that the R_{ct} property is not only sensitive to coverage but also the length that affects the accumulation of charge at the DNA–electrode interface. Overall, the results suggest that the surface coverage is also a function of TNR sequence context, which can be significantly distinct for different TNRs of the same length and for a specific TNR of different lengths.

Preparation of biocompatible films on ultra-flat gold surfaces provides a detailed topographic characterization and the electronic properties of the surface, as recently achieved using single crystalline gold nanoplates.[29,30] To investigate if TNR sequence context or helical flexibility affect the unique structure of the films, topographic images of dsTNR-8 films from three flexibility groups were obtained on ultra-flat gold surfaces (roughness RMS = 0.36 nm) using tapping mode AFM under air dry conditions (Fig. 3). Previously, AFM images were reported for surface-adsorbed strands of TNR sequences to study the molecular junctions in an ~271 bp long sequence.[4] For the first time, this report compares the topographic images of the TNR monolayers prepared on ultra-flat gold substrates. All three sequences appear to be well-uniform and closely

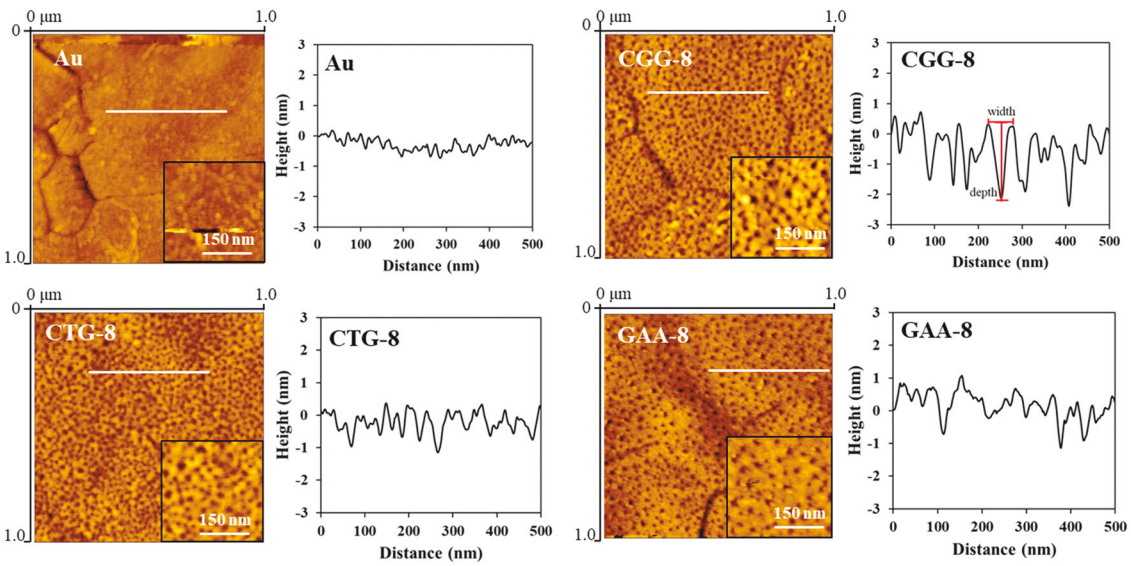

Fig. 3 Tapping mode-AFM images of 1 µm × 1 µm area and line profile of bare ultra-flat gold substrate and surface-tethered films of double-stranded CGG-8, CTG-8, and GAA-8. The white line in the images represents the region of the extracted line profile of 500 nm length. The inset images in the black borders are high resolution images (300 nm × 300 nm) of the surfaces. Black spots in the image are pinholes in TNR films and appear as inverted peaks in the extracted profiles. The red measurement lines in the CGG-8 profile represent the depth and width of an assumed pinhole. Height images are provided in the ESI.†

Table 3 The average values of surface parameters extracted from surface profile, surface densities, and charge transfer resistance values of dsTNR-8 of the three flexibility groups. Parentheses represent standard deviation of measurements

TNR	Flexibility	Number of pinholes (cm^{-2})	Roughness/pinhole depth (nm)	Pinhole width (nm)	Surface density (10^{12} molecules cm^{-2})	R_{ct} (Ω cm^2)
CGG-8	Highest	1.0×10^{11}	2.3 (0.2)	46 (4)	5.7 (2.2)	3108 (193)
CTG-8	Medium	1.2×10^{11}	1.1 (0.1)	27 (4)	0.2 (0.1)	1497 (179)
GAA-8	Least	0.8×10^{11}	1.6 (0.2)	32 (4)	0.9 (0.5)	1855 (75)

packed, as reported earlier for mixed-sequence double-stranded DNA oligonucleotides of similar length and concentration.[31,32] Despite dense film packing, the TNR molecules protrude from the surface (as shown in the height image given in the ESI,† Fig. S4) with varying heights but by less than the theoretical height of an extended DNA duplex oriented normal to the surface (~9 nm). The height profile suggests the approximate heights of CGG-8 (2.5 nm), CTG-8 (1.2 nm), and GAA-8 (1.8 nm), which also appears to be sequence-specific rather than according to the rank in the flexibility scale. A unique feature that is clearly visible and comparable in the monolayer images is the size and density of pinholes (black spots), creating roughness on the surface compared to the flat bare gold. By extracting the line profiles of each image across 500 nm length (white line), depth (roughness) and width of the so-called 'pinholes' were analysed as labelled on the line profile of CGG-8 (Fig. 3). In addition, pinhole density (#pinholes/cm^2) was calculated by counting the number of pinholes using the images of 300 nm × 300 nm resolution given in the inset of each image in Fig. 3. Table 3 compares the parameters extracted from the surface profile, surface densities, and charge transfer resistance values of TNR-8 of the three flexibility groups. Overall, CGG-8 (highly flexible) has a lower number of pinholes but the highest roughness, pinhole width, surface density, and R_{ct}. In contrast, the medium flexible CTG-8 carries the highest number of pinholes but the lowest roughness, pinhole width, surface density, and R_{ct}. The least flexible sequence of GAA-8 has the lowest number of pinholes while it remains in between the two groups for other properties. The extracted parameters from the topographic images confirm the sequence-dependence of the monolayer properties.

Charge transport through DNA has been a hot area for nanoelectronics and bioelectronics application.[33,34] However, the challenge has been the variety of factors profoundly affecting DNA conductivity.[35] Probing the electrical conductance of DNA has resulted in the discovery of a variety of electrical behaviours, such as insulating,[36,37] semiconducting,[38,39] and metal-like conducting.[40,41] Surface adsorbed DNA molecules with heights of ~2.4 nm were reported to be electrically conductive.[41] This was attributed to the fact that the height corresponds to the diameter of B-DNA that may promote charge transport through an ordered π-stacked pathway. Whereas, DNA molecules having 1.1 nm height behaved as insulators, perhaps due to the disruption of the B-DNA structure that diminishes the π-stack interactions between neighbouring base pairs. Further, DNA structures comprising long double strands, poly (G)–poly (C), tetra molecular G4-DNA molecules, chemically modified DNA, and hybrid metal–DNA complex were reported to be more conductive than bare dsDNA.[42] Here, we investigated the sequence-dependent effect of TNRs on their electrical conductivity through C-AFM measurements in air in contact mode between ±2 V. Fig. 4 shows the *I–V* curves of the bare gold substrate, and dsCCG-8, dsCTG-8, and dsGAA-8 films. The gold substrate was found to be highly conductive where the current reached saturation at 10 nA, as reported previously,[35] which confirms that the gold surface is highly clean and polished. To investigate the conductivities of dsTNR-8, several loading forces were applied to make a contact between TNR and the tip using setpoint potentials of 0.1–0.5 V (17–85 nN). This is because applying a high force in the beginning may deform the films. The CGG-8 sequence was found to be non-conductive in the range of 17–50 nN loading force and highly conductive like the gold substrate when a force beyond 68 nN was applied. Previously, Salmeron and co-workers observed a stepwise increase in current with applied loading force across a 1-hexadecanethiol (~2 nm) monolayer on a gold surface.[43] The same group also observed that the same load has different effects on the current response of different molecules due to different adhesion forces existing between the sample and tip.[44]

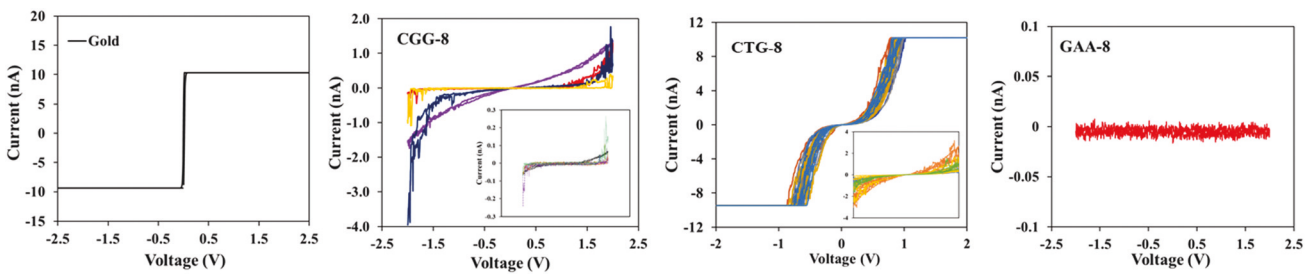

Fig. 4 Current–voltage (*I–V*) curves of the bare gold surface, and double-stranded CGG-8, CTG-8 and GAA-8 repeats. The insets for the CGG-8 and CTG-8 sequences show the lower current regime at the pinholes of the sequence. At least five various spots were used to measure the conductivity of these sequences.

In light of the past studies, we assume that a large adhesion force exists between the TNR samples and tip at a loading force >68 nN that perhaps causes penetration through the monolayer and direct contact between the tip and gold substrate. Here, quantifying the effect of such contributing factors is beyond the scope of the work. After optimizing the loading force, 68 nN was set constant to collect the *I–V* curves of the TNR sequences. Previously, a similar strategy was used where dsDNA was chemically bonded to a gold substrate but the contact between dsDNA and the tip was physical, which produced a current less than 1 nA for a similar length of sequences.[45] For CGG-8, the current was found to be higher than 1 nA at various spots (5 different spots) with slight differences. Moreover, a one order of magnitude lower current was also observed around the pinhole locations, shown in the inset of CGG-8, which is attributed to poor contact between the DNA and the tip at those locations as observed previously.[45,46] Unexpectedly, CTG-8 was found to be 10× more conductive than CGG-8 with current >10 nA, while one order of magnitude lower currents were observed at the pinhole locations, as shown in the inset. These results are unexpected because such high currents for such a sequence, size, film height, and without a chemical bridge between tip and DNA have not been reported before. The electrical conductivity of CTG-8 is aligned with the electrochemical impedance response, where CTG-8 is least resistive compared to the other TNR-8. On the other hand, GAA-8 was found to be an insulator regardless of the location of measurements. One reason may be that it is an AT-rich sequence and it has been reported that the insertion of A–T basepairs into GC-rich sequences decreases conductance exponentially with the length of A–T basepairs with a decay constant of 0.43 $Å^{-1}$.[47] Nevertheless, the signature confirms the sequence-dependent conductive properties of the TNRs. It is important to note here that inhomogeneity and thus variance in electrical conduction of DNA films due to terraces and atomic steps of ultra-flat Au(111) surfaces, having roughness RMS $\approx$ 0.32–0.36 nm, have not been a matter of concern in the previous reports.[31,45,48,49] We believe that this is because of the large difference in the dimensions of the DNA molecule and surface defects. Moreover, using a high concentration (*e.g.* 5–10 μM) and incubation time of 24–48 hours enables a tightly packed film, as shown Fig. 3. Therefore, we ruled this out as a potential problem in our current measurements considering the present experimental conditions.

4. Conclusions

We investigated here the effect of sequence context and flexibility of three disease-relevant trinucleotide repeat sequences on their monolayer properties. The sequences of the three flexibility groups showed distinct electrochemical, electrical, and surface properties, which were found to be sequence-dependent rather than dependent on the reported flexibility rank. The trends of R_{ct} and surface densities were similar for dsTNR-8, showing their direct correlation. Nevertheless, the R_{ct} property was also found to be sensitive to the length and charge of the DNA sequence, therefore this property may be useful for designing a biosensing platform to detect few but very long repeat sequences. Topographically, it was clear that despite having the same base-pair lengths at the molecular level, the surface-tethered films of repeats adopted a unique structure directed by their sequence. The electrical conductance results proved that a film height less than 2.4 nm can also be conductive without even having a chemical bridge, therefore sequence dependence may be an appropriate parameter to explain the behaviour. Thus, the unique responses of the TNRs studied here will be useful in the design of biosensing platforms for fatal neurodegenerative diseases as well as giving a new direction for the bioelectronics field in the future.

Conflicts of interest

There are no conflicts to declare.

Acknowledgements

The authors acknowledge Prof. Yi Lu from the University of Illinois Urbana-Champaign for his useful suggestions on the manuscript. We also acknowledge Dr. Kathy Walsh at Material Research Laboratory, University of Illinois at Urbana-Champaign Illinois. ''Atomic force microscopy imaging was carried out in part in the Materials Research Laboratory Central Research Facilities, University of Illinois.'' MHS acknowledges National Science Foundation grant #1940716 to partly fund the project.

References

1 M. Mitas, Trinucleotide repeats associated with human disease, *Nucleic Acids Res.*, 1997, **25**(12), 2245–2254.
2 K. J. Rohilla and K. T. Gagnon, RNA biology of disease-associated microsatellite repeat expansions, *Acta Neuropathol. Commun.*, 2017, **5**(1), 63.
3 A. Kiliszek and W. Rypniewski, Structural studies of CNG repeats, *Nucleic Acids Res.*, 2014, **42**(13), 8189–8199.
4 R. R. Sinden, V. N. Potaman, E. A. Oussatcheva, C. E. Pearson, Y. L. Lyubchenko and L. S. Shlyakhtenko, Triplet repeat DNA structures and human genetic disease: dynamic mutations from dynamic DNA, *J. Biosci.*, 2002, **27**(1), 53–65.
5 P. Baldi and P. F. Baisnee, Sequence analysis by additive scales: DNA structure for sequences and repeats of all lengths, *Bioinformatics*, 2000, **16**(10), 865–889.
6 R. Gellibolian, A. Bacolla and R. D. Wells, Triplet repeat instability and DNA topology: an expansion model based on statistical mechanics, *J. Biol. Chem.*, 1997, **272**(27), 16793–16797.
7 P. D. Chastain and R. R. Sinden, CTG repeats associated with human genetic disease are inherently flexible, *J. Mol. Biol.*, 1998, **275**(3), 405–411.
8 M. Gomes-Pereira and D. G. Monckton, Ethidium Bromide Modifies The Agarose Electrophoretic Mobility of CAG·CTG

Alternative DNA Structures Generated by PCR, *Front. Cell. Neurosci.*, 2017, **11**, 153.

9 P. D. Chastain, E. E. Eichler, S. Kang, D. L. Nelson, S. D. Levene and R. R. Sinden, Anomalous Rapid Electrophoretic Mobility of DNA Containing Triplet Repeats Associated with Human Disease Genes, *Biochemistry-Us*, 1995, **34**(49), 16125–16131.

10 M. Malgowska, D. Gudanis, R. Kierzek, E. Wyszko, V. Gabelica and Z. Gdaniec, Distinctive structural motifs of RNA G-quadruplexes composed of AGG, CGG and UGG trinucleotide repeats, *Nucleic Acids Res.*, 2014, **42**(15), 10196–10207.

11 K. Sobczak, G. Michlewski, M. de Mezer, E. Kierzek, J. Krol, M. Olejniczak, R. Kierzek and W. J. Krzyzosiak, Structural Diversity of Triplet Repeat RNAs, *J. Biol. Chem.*, 2010, **285**(17), 12755–12764.

12 M. Zheng, X. Huang, G. K. Smith, X. Yang and X. Gao, Genetically Unstable CXG Repeats are Structurally Dynamic and Have a High Propensity for Folding. An NMR and UV Spectroscopic Study, *J. Mol. Biol.*, 1996, **264**(2), 323–336.

13 E. M. LeProust, C. E. Pearso, R. R. Sinden and X. Gao, Unexpected formation of parallel duplex in GAA and TTC trinucleotide repeats of Friedreich's ataxia, *J. Mol. Biol.*, 2000, **302**(5), 1063–1080.

14 A. M. Paiva and R. D. Sheardy, Influence of Sequence Context and Length on the Structure and Stability of Triplet Repeat DNA Oligomers, *Biochemistry*, 2004, **43**(44), 14218–14227.

15 J. Huang and S. Delaney, Unique Length-Dependent Biophysical Properties of Repetitive DNA, *J. Phys. Chem. B*, 2016, **120**(18), 4195–4203.

16 A. Z. Qamar, N. Asefifeyzabadi, M. Taki, S. Naphade, L. M. Ellerby and M. H. Shamsi, Characterization and application of fluidic properties of trinucleotide repeat sequences by wax-on-plastic microfluidics, *J. Mater. Chem. B*, 2020, **8**(4), 743–751.

17 A. N. Rao and D. W. Grainger, Biophysical Properties Of Nucleic Acids At Surfaces Relevant To Microarray Performance, *Biomater. Sci.*, 2014, **2**(4), 436–471.

18 M. Taki, K. J. Rohilla, M. Barton, M. Funneman, N. Benzabeh, S. Naphade, L. M. Ellerby, K. T. Gagnon and M. H. Shamsi, Novel probes for label-free detection of neurodegenerative GGGGCC repeats associated with amyotrophic lateral sclerosis, *Anal. Bioanal. Chem.*, 2019, **411**(26), 6995–7003.

19 L. Au, B. Lim, P. Colletti, Y.-S. Jun and Y. Xia, Synthesis of Gold Microplates Using Bovine Serum Albumin as a Reductant and a Stabilizer, *Chem. – Asian J.*, 2010, **5**(1), 123–129.

20 A. B. Steel, T. M. Herne and M. J. Tarlov, Electrochemical Quantitation of DNA Immobilized on Gold, *Anal. Chem.*, 1998, **70**(22), 4670–4677.

21 http://gwyddion.net/.

22 P. V. Jithesh, P. Singh and R. Joshi, Molecular dynamics studies of trinucleotide repeat DNA involved in neurodegenerative disorders, *J. Biomol. Struct. Dyn.*, 2001, **19**(3), 479–495.

23 J. Kafka, O. Pänke, B. Abendroth and F. Lisdat, A label-free DNA sensor based on impedance spectroscopy, *Electrochim. Acta*, 2008, **53**(25), 7467–7474.

24 M. N. Alam, M. H. Shamsi and H.-B. Kraatz, Scanning positional variations in single-nucleotide polymorphism of DNA: an electrochemical study, *Analyst*, 2012, **137**(18), 4220–4225.

25 M. H. Shamsi and H.-B. Kraatz, Electrochemical signature of mismatch in overhang DNA films: a scanning electrochemical microscopic study, *Analyst*, 2013, **138**(12), 3538–3543.

26 M. H. Shamsi and H.-B. Kraatz, The effects of oligonucleotide overhangs on the surface hybridization in DNA films: an impedance study, *Analyst*, 2011, **136**(15), 3107–3112.

27 M. Riedel, J. Kartchemnik, M. J. Schöning and F. Lisdat, Impedimetric DNA Detection—Steps Forward to Sensorial Application, *Anal. Chem.*, 2014, **86**(15), 7867–7874.

28 A. B. Steel, R. L. Levicky, T. M. Herne and M. J. Tarlov, Immobilization of Nucleic Acids at Solid Surfaces: Effect of Oligonucleotide Length on Layer Assembly, *Biophys. J.*, 2000, **79**(2), 975–981.

29 Y. Yoo, H. Lee, H. Lee, M. Lee, S. Yang, A. Hwang, S.-I. Kim, J. Y. Park, J. Choo, T. Kang and B. Kim, Surfactant-Free Vapor-Phase Synthesis of Single-Crystalline Gold Nanoplates for Optimally Bioactive Surfaces, *Chem. Mater.*, 2017, **29**(20), 8747–8756.

30 W. Jeong, M. Lee, H. Lee, H. Lee, B. Kim and J. Y. Park, Ultraflat Au nanoplates as a new building block for molecular electronics, *Nanotechnology*, 2016, **27**(21), 215601.

31 C. Nogues, S. R. Cohen, S. S. Daube and R. Naaman, Electrical properties of short DNA oligomers characterized by conducting atomic force microscopy, *Phys. Chem. Chem. Phys.*, 2004, **6**(18), 4459–4466.

32 D. Erts, B. Polyakov, H. Olin and E. Tuite, Spatial and mechanical properties of dilute DNA monolayers on gold imaged by AFM, *J. Phys. Chem. B*, 2003, **107**(15), 3591–3597.

33 R. Korol and D. Segal, From Exhaustive Simulations to Key Principles in DNA Nanoelectronics, *J. Phys. Chem. C*, 2018, **122**(8), 4206–4216.

34 J. C. Genereux and J. K. Barton, Mechanisms for DNA charge transport, *Chem. Rev.*, 2010, **110**(3), 1642–1662.

35 K. L. Jiménez-Monroy, N. Renaud, J. Drijkoningen, D. Cortens, K. Schouteden, C. van Haesendonck, W. J. Guedens, J. V. Manca, L. D. A. Siebbeles, F. C. Grozema and P. H. Wagner, High Electronic Conductance through Double-Helix DNA Molecules with Fullerene Anchoring Groups, *J. Phys. Chem. A*, 2017, **121**(6), 1182–1188.

36 P. J. de Pablo, F. Moreno-Herrero, J. Colchero, J. Gómez Herrero, P. Herrero, A. M. Baró, P. Ordejón, J. M. Soler and E. Artacho, Absence of dc-Conductivity in λ-DNA, *Phys. Rev. Lett.*, 2000, **85**(23), 4992–4995.

37 A. J. Storm, J. v. Noort, S. d. Vries and C. Dekker, Insulating behavior for DNA molecules between nanoelectrodes at the 100 nm length scale, *Appl. Phys. Lett.*, 2001, **79**(23), 3881–3883.

38 D. Porath, A. Bezryadin, S. de Vries and C. Dekker, Direct measurement of electrical transport through DNA molecules, *Nature*, 2000, **403**(6770), 635–638.

39 H. Watanabe, C. Manabe, T. Shigematsu, K. Shimotani and M. Shimizu, Single molecule DNA device measured with triple-probe atomic force microscope, *Appl. Phys. Lett.*, 2001, **79**(15), 2462–2464.

40 C. J. Murphy, M. R. Arkin, Y. Jenkins, N. D. Ghatlia, S. H. Bossmann, N. J. Turro and J. K. Barton, Long-range

photoinduced electron transfer through a DNA helix, *Science*, 1993, **262**(5136), 1025–1029.

41 A. Y. Kasumov, D. V. Klinov, P.-E. Roche, S. Guéron and H. Bouchiat, Thickness and low-temperature conductivity of DNA molecules, *Appl. Phys. Lett.*, 2004, **84**(6), 1007–1009.

42 R. Zhuravel, A. Stern, N. Fardian-Melamed, G. Eidelshtein, L. Katrivas, D. Rotem, A. B. Kotlyar and D. Porath, Advances in Synthesis and Measurement of Charge Transport in DNA-Based Derivatives, *Adv. Mater.*, 2018, **30**(41), 1706984.

43 Y. Qi, I. Ratera, J. Y. Park, P. D. Ashby, S. Y. Quek, J. B. Neaton and M. Salmeron, Mechanical and Charge Transport Properties of Alkanethiol Self-Assembled Monolayers on a Au(111) Surface: The Role of Molecular Tilt, *Langmuir*, 2008, **24**(5), 2219–2223.

44 L. Fang, J. Y. Park, H. Ma, A. K. Y. Jen and M. Salmeron, Atomic Force Microscopy Study of the Mechanical and Electrical Properties of Monolayer Films of Molecules with Aromatic End Groups, *Langmuir*, 2007, **23**(23), 11522–11525.

45 H. Cohen, C. Nogues, D. Ullien, S. Daube, R. Naaman and D. Porath, Electrical characterization of self-assembled single- and double-stranded DNA monolayers using conductive AFM, *Faraday Discuss.*, 2006, **131**, 367–376.

46 A. Salomon, D. Cahen, S. Lindsay, J. Tomfohr, V. B. Engelkes and C. D. Frisbie, Comparison of electronic transport measurements on organic molecules, *Adv. Mater.*, 2003, **15**(22), 1881–1890.

47 B. Xu, P. Zhang, X. Li and N. Tao, Direct Conductance Measurement of Single DNA Molecules in Aqueous Solution, *Nano Lett.*, 2004, **4**(6), 1105–1108.

48 L. Cai, H. Tabata and T. Kawai, Probing electrical properties of oriented DNA by conducting atomic force microscopy, *Nanotechnology*, 2001, **12**(3), 211–216.

49 H. Cohen, C. Nogues, R. Naaman and D. Porath, Direct measurement of electrical transport through single DNA molecules of complex sequence, *Proc. Natl. Acad. Sci. U. S. A.*, 2005, **102**(33), 11589–11593.